Extended object tracking based on superellipses

Lin Gao*, Giorgio Battistelli§, and Luigi Chisci§
*School of Information and Communication Engineering
University of Electronic Science and Technology of China
Email: lingao_1014@126.com
§Dipartimento di Ingegneria dell'Informazione (DINFO)
Università degli Studi di Firenze
Email: {giorgio.battistelli, luigi.chisci}@unifi.it

***Abstract*—This paper presents an approach for 2-dimensional *extended object tracking* (EOT). The extended object (EO) is represented as a superellipse characterized by kinematic and shape states, with the latter uniquely specified in terms of four parameters. An approximated measurement model is proposed accounting for the fact that the measurements can be generated from any position inside or on the contour of the EO. Then, EOT is performed by iteratively estimating the kinematic state via a Kalman filter, while the posterior of the shape state is represented and propagated in particle filter form due to the strong nonlinearity of the resulting shape measurement model. Simulation results are provided to assess the performance of the proposed method.**

***Index Terms*—Superellipse, extended object tracking, Kalman filter, particle filter.**

I. Introduction

Over the last decade, a lot of work has been devoted to *extended object tracking* (EOT) [1] due to the rapid advances of high-resolution sensor technology. Unlike traditional point object tracking wherein the object of interest produces at most one measurement at each time, an *extended object* (EO) normally occupies several sensor resolution cells so that multiple measurements can be extracted at each observation. In addition to estimation of the kinematic state, which describes the motion of the EO center, it is also important to perform shape estimation, which represents a further challenge with respect to point object tracking. To this end, an appropriate shape model, which summarizes shape information into a few parameters, is first needed. Then, shape estimation can be recast into estimation of such parameters from data following, e.g., a Bayesian approach.

Up to date, the most commonly used shapes for 2-dimensional EOs are ellipses [2] and rectangles [3], which require only three parameters (i.e., rotation angle and lengths of the axes), so that EOT can be carried out with fast and tidy algorithms. A milestone of elliptical EOT traces back to [4], where a *random matrix* (RM) is adopted to represent an elliptical EO. With such a model, a Kalman filter-based approach is proposed for EOT. However, such a method relies on the assumption that the measurement error caused by noise is negligible. Such an assumption is relaxed in the subsequent work [5]. Moreover, a variational Bayesian EOT method [6] is also proposed, which has the potential of tolerating larger measurement noise compared to the work of [4], [5]. Since with the RM representation the rotation angle of the EO is not directly available, in [7] a more refined RM model is proposed to consider the EO orientation with a symmetric positive definite matrix. Later, the orientation angle is explicitly taken into consideration as a new variable in the RM-based approach, and the variational Bayesian inference method is developed for EOT [8]. More recently, under the assumption that the measurements arise only from the boundary of the object, a Bayesian Wishart filter has been proposed for tracking the random EO shape [9]. In contrast to the RM-based approach, [10] proposes to explicitly model the shape of an elliptical EO with three parameters, i.e. the lengths of the two axes and the orientation angle. Then, an extended Kalman filter approach, separately performing kinematic and shape state estimation, can be exploited.

Nevertheless, an ellipse cannot adequately describe complex shapes, thus cannot be applied to EOT where details of the EO shape are required. For modeling irregular EO shapes, a possible strategy is to adopt multiple ellipses, each representing a part of the EO [11]. In this way, EOT algorithms for generally-shaped EOs can be obtained by extending the aforementioned elliptical methods. Furthermore, principled shape modeling can be accomplished by describing the EO contour by, e.g.: (1) a Gaussian process based on the discretization of a radial function [12]; (2) a random hypersurface which adopts a convex-star set [13], [14], [15]; (3) control point-based models such as spline curves [16] or deformation of reference points [17]. In particular, in the random hypersurface-based methods, the radius function of the EO shape is parameterized with Fourier coefficients, thus allowing an efficient implementation for the Gaussian-assumed Bayesian state estimator. The common drawback of these methods is that normally a large number of parameters is needed in order to accurately model the EO shape, thus increasing the dimension of the shape state vector. Furthermore, EOT performance deteriorates whenever the number of available measurements produced by the EO gets smaller.

In this paper, we propose to model the EO shape by means of a superellipse [18], which represents a generalization of the ellipse. Compared to the elliptical model, an additional squareness parameter is involved to model the EO shape. The superellipse has been widely used in the field of image-based static object shape recovery [19], [20], [21]. However

the considered EOT problem differs from image-based shape recovery mainly in two aspects. The first and most important one is that in image-based shape recovery, measurements are produced only on the contour of the object, while in EOT measurements can also fall inside the EO. Moreover, EOT also aims to recursively estimate the kinematic state of the object, which is clearly not of interest in image-based shape recovery.

In our work, the EO is represented via both kinematic and shape states, where the kinematic state can be directly estimated via a Kalman filter. Then, an approximated measurement function, which accounts for the fact that measurements can be generated from any position (inside or on the contour) of the 2-dimensional EO, is proposed. Due to the strong nonlinearity of the shape measurement model, a Monte Carlo approach is followed by representing the shape posterior via a set of particles and, accordingly, shape estimation is carried out by means of a particle filter [24]. The performance of the proposed superellipse-based EOT method is verified via simulations.

The rest of this paper is organized as follows. Section II provides background on superellipse-based EO representation. Next, section III introduces the proposed algorithm. The evaluation of the proposed method is provided in Section IV. Finally, section V ends the paper with conclusions.

II. Superellipse-based EO representation

A. Motivations

Most of the existing work on EOT relies on modeling the EO to be tracked as either an ellipse [2] or a rectangle [3], thus leading to simple, closed-form and tractable EOT algorithms. The major limitation of this work is that the employed EO model cannot provide shape details. For irregular shape EO tracking, multi-ellipse, convex-star, and Gaussian process-based models can be adopted. These models, however, normally involve a large number of parameters to represent the EO shape, with consequent performance degradation when applied to EOs that produce few measurements. In this respect, the goal of this work is to adopt a model that is able to: 1) describe a larger class of EO shapes including elliptical/rectangular ones; 2) involve a few parameters. These requirements have led us to the superellipse model.

Superellipses have been widely exploited to represent the object shape in a variety of fields, such as forestry [26], [27], medical modeling [28], computer vision [29], aircraft modeling [30], and so on. Notice that the superellipse model just needs an extra scalar parameter, called *squareness*, with respect to ellipse/rectangle models but, thanks to such a parameter, can be used to represent a much larger set of shapes including rectangles, ellipses and also non-convex shapes. More importantly, the superellipse model can be further extended to model a broader class of object shapes with additional (e.g., tapering and bending) parameters. For the above reasons, this paper is devoted to EOT based on superellipse modeling of the EO.

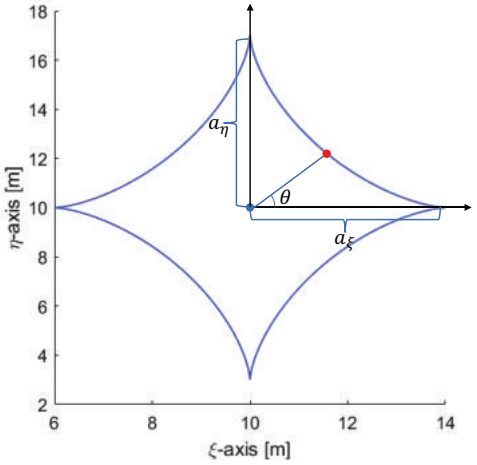

Fig. 1: Superellipse with $\varepsilon = 4$, $a_\xi = 4\,[m]$ and $a_\eta = 7\,[m]$.

B. Superellipse model

A superellipse, centered at the origin of a 2D Cartesian coordinate system $O\xi\eta$ and with axes aligned to the coordinate axes, can be uniquely characterized via the following inside-outside function:

$$F(\xi, \eta, a_\xi, a_\eta, \varepsilon) = \left(\frac{\xi}{a_\xi}\right)^{\frac{2}{\varepsilon}} + \left(\frac{\eta}{a_\eta}\right)^{\frac{2}{\varepsilon}}, \tag{1}$$

where: (ξ, η) is the position of a point in $O\xi\eta$; a_ξ, a_η are the lengths of the two semi-axes; ε is a squareness parameter satisfying $\varepsilon > 0$ ($\varepsilon = 1$ corresponding to the special case of an ellipse). The inside-outside function is such that:

- $F(\xi, \eta, a_\xi, a_\eta, \varepsilon) > 1$, if (ξ, η) is outside the superellipse;
- $F(\xi, \eta, a_\xi, a_\eta, \varepsilon) = 1$, if (ξ, η) is on the superellipse;
- $F(\xi, \eta, a_\xi, a_\eta, \varepsilon) < 1$, if (ξ, η) is inside the superellipse.

The parametric form of a superellipse is given by

$$\xi = a_\xi\, f_c\,(\varepsilon, \theta)\,, \quad \eta = a_\eta\, f_s\,(\varepsilon, \theta)\,, \tag{2}$$

where θ is the angle of the vector $[\xi, \eta]^\top$ with respect to the positive ξ-direction, and

$$f_c\,(\varepsilon, \theta) = |\cos\theta|^\varepsilon \operatorname{sgn}(\cos\theta), \tag{3}$$

$$f_s\,(\varepsilon, \theta) = |\sin\theta|^\varepsilon \operatorname{sgn}(\sin\theta). \tag{4}$$

As it can be seen, we have

$$\frac{f_s\,(\varepsilon, \theta)}{f_c\,(\varepsilon, \theta)} = |\tan\theta|^\varepsilon \operatorname{sgn}(\tan\theta). \tag{5}$$

An example of superellipse is illustrated in Fig. 1. In order to give an idea on how the superellipse can represent different shapes of EO, we show the resulting geometry of the superellipse for different values of ε in Fig. 2.

C. EO representation by superellipse

For EOT purposes, besides shape, also position and orientation of the EO need to be estimated. In this paper, two vectors

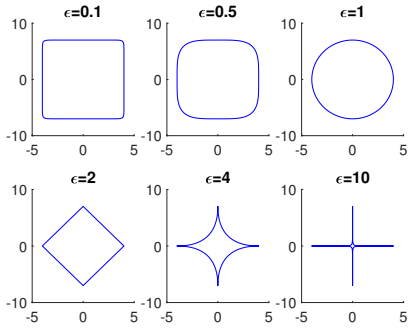

Fig. 2: Geometry of superellipse versus ε (for $a_\xi = 4\,[m]$ and $a_\eta = 7\,[m]$).

are adopted to model the 2D EOT, i.e., the kinematic state x of the EO center and shape state s defined as follows:

$$x \triangleq [\underbrace{\xi_o, \eta_o}_{\text{position}}, \underbrace{\dot{\xi}_o, \dot{\eta}_o}_{\text{velocity}}]^\top \tag{6}$$

$$s \triangleq [\underbrace{a_\xi, a_\eta}_{\text{semi-axis lengths}}, \underbrace{\alpha}_{\text{rotation angle}}, \underbrace{\varepsilon}_{\text{squareness}}]^\top. \tag{7}$$

where: (ξ_o, η_o) and $(\dot{\xi}_o, \dot{\eta}_o)$ denote position and velocity of the EO center, respectively; α characterizes the orientation of the EO. Hereafter, for the sake of simplicity, it is assumed that the transition functions for x and s are both linear, i.e.,

$$x_t = A_t^x x_{t-1} + w_t^x, \tag{8}$$

$$s_t = A_t^s s_{t-1} + w_t^s, \tag{9}$$

where w_t^x and w_t^s are zero-mean white Gaussian process disturbances with covariances Q_t^x and Q_t^s, respectively. It is worth noting that the proposed method can be easily extended to the case of nonlinear state transition models.

In the context of 2D EOT, available measurements can be regarded as generated from any point that is either inside or on the contour of the EO. For any noisy measurement z generated by a superelliptical EO, it can therefore be assumed that there exist a scalar $l \in [-1, 1]$ and angle $\theta \in [-\frac{\pi}{2}, \frac{\pi}{2}]$, such that

$$z \triangleq \begin{bmatrix} \xi_v \\ \eta_v \end{bmatrix} = \begin{bmatrix} \xi_o \\ \eta_o \end{bmatrix} + T(\alpha) \begin{bmatrix} a_\xi\, f_c\,(\varepsilon, \theta) \\ a_\eta\, f_s\,(\varepsilon, \theta) \end{bmatrix} l + v, \tag{10}$$

where $v \sim \mathcal{N}(\cdot; 0, R)$ is a Gaussian random variable with zero mean and covariance R, and

$$T(\alpha) = \begin{bmatrix} \cos\alpha & -\sin\alpha \\ \sin\alpha & \cos\alpha \end{bmatrix} \tag{11}$$

is the rotation matrix associated to α. At each observation of the EO, a random number $M \sim \text{Poisson}(\lambda_z)$ of measurements z_i $(i = 1, \ldots, M)$ of the form (10) (for unknown values of l, α, v) are generated.

III. The Proposed Algorithm

A. Approximated likelihood for shape estimation

The key issue for designing a 2D EOT algorithm is to suitably define a likelihood function that allows to measure how likely an EO state (x, s) is, given the available measurement set $Z = \{z_1, \ldots, z_M\}$. Due to the fact that the dynamic models of kinematic state x and shape state s are supposed to be independent in this paper (actually such an assumption has been exploited in several other existing works, e.g., [4], [10]), this subsection will focus only on shape estimation. Moreover, since the kinematic state can be easily and independently obtained via a *Kalman filter* (KF), it is temporarily supposed to be known in this subsection.

In order to derive the likelihood for shape estimation, let us rewrite the measurement equation (10) as follows:

$$\begin{aligned} \begin{bmatrix} \bar{\xi}_v \\ \bar{\eta}_v \end{bmatrix} &\triangleq z - \begin{bmatrix} \xi_o \\ \eta_o \end{bmatrix} \\ &= \begin{bmatrix} \cos\alpha & -\sin\alpha \\ \sin\alpha & \cos\alpha \end{bmatrix} \begin{bmatrix} a_\xi\, f_c\,(\varepsilon, \theta) \\ a_\eta\, f_s\,(\varepsilon, \theta) \end{bmatrix} l + v. \end{aligned} \tag{12}$$

Neglecting the unknown zero-mean measurement error v, we have

$$\begin{aligned} &\begin{bmatrix} \bar{\xi}_v \\ \bar{\eta}_v \end{bmatrix} \approx \begin{bmatrix} \cos\alpha & -\sin\alpha \\ \sin\alpha & \cos\alpha \end{bmatrix} \begin{bmatrix} a_\xi\, f_c\,(\varepsilon, \theta) \\ a_\eta\, f_s\,(\varepsilon, \theta) \end{bmatrix} l \\ &\Rightarrow \begin{bmatrix} \cos\alpha & \sin\alpha \\ -\sin\alpha & \cos\alpha \end{bmatrix} \begin{bmatrix} \bar{\xi}_v \\ \bar{\eta}_v \end{bmatrix} \approx \begin{bmatrix} l\, a_\xi\, f_c\,(\varepsilon, \theta) \\ l\, a_\eta\, f_s\,(\varepsilon, \theta) \end{bmatrix} \\ &\Rightarrow \begin{bmatrix} \bar{\xi}_v \cos\alpha + \bar{\eta}_v \sin\alpha \\ -\bar{\xi}_v \sin\alpha + \bar{\eta}_v \cos\alpha \end{bmatrix} \approx \begin{bmatrix} l\, a_\xi\, f_c\,(\varepsilon, \theta) \\ l\, a_\eta\, f_s\,(\varepsilon, \theta) \end{bmatrix} \\ &\Rightarrow \frac{a_\eta\, f_s\,(\varepsilon, \theta)}{a_\xi\, f_c\,(\varepsilon, \theta)} \approx \frac{-\bar{\xi}_v \sin\alpha + \bar{\eta}_v \cos\alpha}{\bar{\xi}_v \cos\alpha + \bar{\eta}_v \sin\alpha}. \end{aligned} \tag{13}$$

Notice that the above approximation is justified by the fact that the measurement error v, besides being zero-mean, should have covariance R not too large compared to the EO size in order to allow reasonable shape and size estimation from the available measurements irrespectively of the used approach. Then, substituting (5) into (13), we have

$$\frac{a_\eta}{a_\xi} |\tan\theta|^\varepsilon \text{sgn}(\tan\theta) \approx \frac{-\bar{\xi}_v \sin\alpha + \bar{\eta}_v \cos\alpha}{\bar{\xi}_v \cos\alpha + \bar{\eta}_v \sin\alpha}. \tag{14}$$

Next, we get

$$\begin{aligned} \tan\theta \approx \text{sgn}&\left[\frac{a_\xi\left(-\bar{\xi}_v \sin\alpha + \bar{\eta}_v \cos\alpha\right)}{a_\eta\left(\bar{\xi}_v \cos\alpha + \bar{\eta}_v \sin\alpha\right)}\right] \\ &\times \left|\frac{a_\xi\left(-\bar{\xi}_v \sin\alpha + \bar{\eta}_v \cos\alpha\right)}{a_\eta\left(\bar{\xi}_v \cos\alpha + \bar{\eta}_v \sin\alpha\right)}\right|^{\frac{1}{\varepsilon}}. \end{aligned} \tag{15}$$

As a result, we can get an estimate $\widehat{\theta}$ of θ via

$$\begin{aligned} \widehat{\theta} \approx \text{atan}\Bigg\{&\text{sgn}\left[\frac{a_\xi\left(-\bar{\xi}_v \sin\alpha + \bar{\eta}_v \cos\alpha\right)}{a_\eta\left(\bar{\xi}_v \cos\alpha + \bar{\eta}_v \sin\alpha\right)}\right] \\ &\times \left|\frac{a_\xi\left(-\bar{\xi}_v \sin\alpha + \bar{\eta}_v \cos\alpha\right)}{a_\eta\left(\bar{\xi}_v \cos\alpha + \bar{\eta}_v \sin\alpha\right)}\right|^{\frac{1}{\varepsilon}}\Bigg\}. \end{aligned} \tag{16}$$

Substituting $\widehat{\theta}$ back to (10) yields

$$\begin{bmatrix} \bar{\xi}_v \\ \bar{\eta}_v \end{bmatrix} \approx \begin{bmatrix} \cos\alpha & -\sin\alpha \\ \sin\alpha & \cos\alpha \end{bmatrix} \begin{bmatrix} a_\xi\, f_c(\varepsilon, \widehat{\theta}) \\ a_\eta\, f_s(\varepsilon, \widehat{\theta}) \end{bmatrix} l + v. \tag{17}$$

Please notice that, since the measurement points are assumed to be uniformly distributed within the EO area, once $\widehat{\theta}$ is fixed, it is reasonable to approximately assume that l is uniformly distributed over the interval $[-1,1]$, i.e. $p(l|\theta) = \mathcal{U}(-1,1)$. Following [10], we can further approximate the uniform distribution $\mathcal{U}(-1,1)$ by a zero-mean Gaussian one with suitable variance σ^2. Hence, by defining $\overline{z} = z - [\xi_0\ \eta_0]^\top$, from (17) we approximately have

$$\overline{z} \sim \mathcal{N}(\overline{z}; 0, \sigma^2\,\Gamma(s,\overline{z})\,\Gamma^\top(s,\overline{z}) + R), \tag{18}$$

where

$$\Gamma(s,\overline{z}) \triangleq \begin{bmatrix} \cos\alpha & -\sin\alpha \\ \sin\alpha & \cos\alpha \end{bmatrix} \begin{bmatrix} a_\xi\ f_c(\varepsilon,\widehat{\theta}) \\ a_\eta\ f_s(\varepsilon,\widehat{\theta}) \end{bmatrix}. \tag{19}$$

Please notice that Γ in (19) depends on s and $\overline{z}$ since the parameters α, a_ξ and a_η are contained in s while the computation of $\widehat{\theta}$ in (16) involves s and $\overline{z}$.

Hence, the likelihood of the measurement set $Z = \{z_1,\ldots,z_M\}$ can be evaluated as follows

$$\ell\left(\overline{Z}\middle|\, s\right) = \prod_{i=1}^{M} \mathcal{N}\left(\overline{z}_i; 0, \sigma^2\,\Gamma(s,\overline{z}_i)\,\Gamma^\top(s,\overline{z}_i) + R\right) \tag{20}$$

where $\overline{Z} \triangleq \{\overline{z}_1,\ldots,\overline{z}_M\}$ and $\overline{z}_i = z_i - [\xi_o,\eta_o]^\top$ for $i = 1,\ldots,M$.

B. Superellipse based EOT

In this paper, we propose to perform superellipse EOT by estimating the kinematic state via a Kalman filter [31] and the shape state via a particle filter [24], respectively. The resulting superellipse EOT algorithm is summarized in Algorithm 1, where N denotes the number of particles.

Concerning Algorithm 1, we would like first to explain estimation of the EO kinematic state, which is carried out via steps 1 – 5. Please notice that these steps have been decoupled from shape state estimation by considering a linear measurement equation of the form

$$z_t^i = C x_t + \widetilde{v}_t^i \tag{21}$$

where $C = [I_2, 0_2]$ and the term $\widetilde{v}_t^i$ accounts for both the measurement noise and the fact that each measurement can be randomly generated by any point of the EO according to equation (10). In fact, since at each time instant multiple measurements z_t^i, $i = 1,\ldots,M_t$, are generated, the covariance $\widehat{R}_t$ of $\widetilde{v}_t^i$ can be empirically estimated as sample covariance in step 3 of Algorithm 1 without knowledge of the shape state.

As for the particle filter for the estimation of the shape state, we exploit the approximated likelihood (20) derived in the previous section by replacing, in the computation of each $\overline{z}_t^i$, the unknown center position $[\xi_o\,\eta_o]^\top$ with its estimate $[\xi_{o,t|t}\,\eta_{o,t|t}]^\top$ provided by the Kalman filter. Clearly, this introduces an additional uncertainty since we have

$$\begin{aligned} \overline{z}_t^i &= z_i - [\xi_{o,t|t}\,\eta_{o,t|t}]^\top && (22)\\ &= z_i - [\xi_o,\eta_o]^\top + [\widetilde{\xi}_{o,t}\,\widetilde{\eta}_{o,t}]^\top && (23) \end{aligned}$$

where $[\widetilde{\xi}_{o,t}\,\widetilde{\eta}_{o,t}]^\top$ denotes the center position estimation error at time t. Since the center state is achieved via the Kalman filter (see steps 1 – 7 in Algorithm 1), its estimation error can be reasonably quantified by the covariance matrix $P_{t|t}$. To account for such additional uncertainty, the covariance of the likelihood in (20) is enlarged by setting

$$\ell_t\left(\overline{Z}_t\middle|s\right) = \prod_{i=1}^{M} \mathcal{N}\left(\overline{z}_t^i; 0, \sigma^2\Gamma(s,\overline{z}_t^i)\Gamma^\top(s,\overline{z}_t^i) + R + C P_{t|t} C^\top\right). \tag{24}$$

where $C P_{t|t} C^\top$ is the covariance of the center position estimation error computed by the Kalman filter. Moreover, importance sampling (i.e., step 8 in Algorithm 1) must ensure that $\varepsilon > 0$; this can be easily accomplished by re-generating the particle $s_{t|t-1}^j$ whenever $\varepsilon_{t|t-1}^j \le 0$ until the shape parameter ε becomes larger than zero.

Algorithm 1: Superellipse-based EOT

Input: $Z_t = \{z_t^1,\ldots,z_t^{M_t}\}$, $x_{t-1|t-1}$, $P_{t-1|t-1}$, $\{\omega_{t-1|t-1}^j, s_{t-1|t-1}^j\}_{j=1}^N$

1 Perform kinematic state prediction as follows

$$\begin{aligned} x_{t|t-1} &= A_t^x\, x_{t-1|t-1}, \\ P_{t|t-1} &= A_t^x P_{t-1|t-1} (A_t^x)^\top + Q_t^x; \end{aligned}$$

2 Set $x_{t|t}^0 = x_{t|t-1}$ and $P_{t|t}^0 = P_{t|t-1}$;

3 Compute

$$\widehat{z}_t = \frac{1}{M_t}\sum_{i=1}^{M_t} z_t^i, \quad \widehat{R}_t = \frac{1}{M_t}\sum_{i=1}^{M_t} (z_t^i - \widehat{z}_t)(z_t^i - \widehat{z}_t)^\top;$$

4 **for** $i = 1,\ldots,M_t$ **do**

5 Perform measurement-wise update as follows

$$\begin{aligned} x_{t|t}^i &= x_{t|t}^{i-1} + K_t^i (z_t^i - C x_{t|t}^{i-1}), \\ P_{t|t}^i &= P_{t|t}^{i-1} - K_t^i C P_{t|t}^{i-1}, \\ K_t^i &= P_{t|t}^{i-1} C \left[C P_{t|t}^{i-1} (C)^\top + \widehat{R}_t\right]^{-1}, \end{aligned}$$

6 **end**

7 Set $x_{t|t} = x_{t|t-1}^{M_t}$ and $P_{t|t} = P_{t|t-1}^{M_t}$;

8 Perform importance sampling $s_{t|t-1}^j \sim \mathcal{N}(\cdot; A_t^s \cdot s_{t-1|t-1}^j, Q_t^s)$, $\omega_{t|t-1}^j = \omega_{t-1|t-1}^j$ for $j = 1,\ldots,N$;

9 Set $\overline{Z}_t = \{\overline{z}_t^1,\ldots,\overline{z}_t^{M_t}\}$ with $\overline{z}_t^i$ as in (22) ;

10 Evaluate the likelihood $\ell_t(\overline{Z}_t|\, s_{t|t-1}^j)$ for $j = 1,\ldots,N$;

11 Update particle weights as $\widetilde{\omega}_{t|t}^j \propto \omega_{t|t-1}^j\, \ell_t(\overline{Z}_t|\, s_{t|t-1}^j)$ for $j = 1,\ldots,N$;

12 Let $s_{t|t} = \sum_{j=1}^{N} \widetilde{\omega}_{t|t-1}^j\, s_{t|t-1}^j$;

13 Perform resampling [24] on particle set $\{\widetilde{\omega}_{t|t}^j, s_{t|t-1}^j\}_{j=1}^N$ to produce a new set $\{\omega_{t|t}^j, s_{t|t}^j\}_{j=1}^N$.

Output: $x_{t|t}$, $P_{t|t}$, $s_{t|t}$, $\{\omega_{t|t}^j, s_{t|t}^j\}_{j=1}^N$

Remark 1. *This remark concerns modeling of scalar l in* (17). *As previously pointed out, once the relative angle θ of a measurement with respect to the EO is estimated, the conditional distribution $p(l|\theta)$ is supposed to be uniform within the interval $[-1, 1]$. Clearly this is an approximation since the measurement set Z is no-longer uniformly distributed inside the EO area. However, since such assumption simplifies the likelihood derivation, it is adopted in the proposed algorithm. Extension of the algorithm proposed in this paper to nonuniformly distributed measurements [22], [23] is left as possible future work.*

Remark 2. *This remark concerns the exact likelihood for superellipse based EOT. The exact model for generating a measurement point z is given as follows. First, select a random point p uniformly distributed over the superellipse EO region $\mathcal{R}(s)$ given the EO shape parameter s, then z is obtained by perturbing p with a random Gaussian measurement error v that is independent of p, i.e.*

$$\begin{cases} z &= p + v \\ p &= \mathcal{U}\left(\mathcal{R}(s)\right) \\ v &= \mathcal{N}(0, R) \end{cases}, \tag{25}$$

where $\mathcal{U}(\mathcal{R})$ stands for uniformly distributed random variable over $\mathcal{R}$. Hence, by the independence of p and v, the single-measurement likelihood $\ell(\overline{z}|s)$ turns out to be given by the convolution of the conditional PDF $f_{p|s}(\cdot)$ by the measurement error PDF $f_v(\cdot)$, i.e.,

$$\begin{aligned} \ell(z|s) &= \int f_v(z-p)\, f_{p|s}(p)\, dp \\ &= \frac{1}{area\left[\mathcal{R}(s)\right]} \int_{\mathcal{R}(s)} \mathcal{N}(p; z, R)\, dp\,, \end{aligned} \tag{26}$$

where $area\left[\mathcal{R}(s)\right]$ is superellipse area calculated as [25, Sec. 2.44]

$$area\left[\mathcal{R}(s)\right] = 2a_\xi\, a_\eta\, \varepsilon\, \mathcal{B}\left(\frac{\varepsilon}{2}, \frac{\varepsilon+2}{2}\right), \tag{27}$$

with $\mathcal{B}(x,y) = \frac{\mathcal{G}(x)\mathcal{G}(y)}{\mathcal{G}(x+y)}$ and $\mathcal{G}(\cdot)$ being the Gamma function. Notice that (26) provides the exact likelihood which, though not computable in closed-form, can be approximated by Monte Carlo integration in the following way:

1) *draw a number N_s of samples from a Gaussian distribution with mean z and covariance R;*
2) *approximate the integral of* (26) *as the number of samples inside the superellipse divided by the total number of samples.*

IV. Simulation results

A. Scenario

In order to assess the performance of the proposed method, we considered the EOT scenario described hereafter. The state transition matrices in (8) and (9) are set to

$$A_t^x = \begin{bmatrix} 1 & 0 & T & 0 \\ 0 & 1 & 0 & T \\ 0 & 0 & 1 & 0 \\ 0 & 0 & 0 & 1 \end{bmatrix}, \quad A_t^s = I_4, \tag{28}$$

where $T = 1[s]$ is the sampling interval. The initial kinematic state vector for the EO is set to $[10[m],\, 10[m]],\, 60[m/s],\, 10[m/s]]^\top$, and the trajectory is randomly generated by involving the process noise. The process noise covariance matrices are set to

$$Q_t^x = \mathrm{diag}\left(5[m], 5[m], 5[m/s], 5[m/s]\right)^2, \tag{29}$$

$$Q_t^s = \mathrm{diag}\left(0.5[m], 0.5[m], 2[^o], 0.05\right)^2. \tag{30}$$

The semi-axis lengths of the EO are set to $a_\xi = 3\,[m]$ and $a_\eta = 7\,[m]$. The measurement noise covariance is set to $R_t = \sigma_v^2 I_2$ with $\sigma_v = 0.1\,[m]$. The parameter σ in (20) is set to 0.5. Concerning measurement generation in the simulations, we first randomly choose the number of measurements according to the Poisson distribution. Then, each measurement is generated via the following three steps.

1) Take a rectangle that covers the EO.
2) Uniformly generate a measurement inside the rectangle.
3) Check whether the generated measurement falls within the EO area and, if so, accept this measurement and perturb it by an additive Gaussian measurement error; otherwise repeat step 2.

The above steps are carried out until the chosen number of measurements have been gathered.

In our simulations, the state-of-the-art methods in [10] (referred to as MEM-EKF) and [8] (referred to as RM-VB) are also considered for the sake of comparison. Both algorithms have been initialized with semi-axis lengths equal to $5\,[m]$ and rotation angle to 0°. Further, for the proposed method, the initial squareness parameter is set to 1. As a result, the initial EO estimate is a circle. Mean and covariance of the initial shape state are set to $[5[m],\, 5[m],\, 0[^o],\, 1]^\top$ and $\mathrm{diag}(9[m^2],\, 9[m^2],\, 1[^{o^2}],\, 2)$, respectively. In what follows, the proposed algorithm is referred to as *superellipse-based EOT* (SE-EOT).

The algorithms have been programmed based on MATLAB 2021a launched on a desktop with CPU Ryzen 7 5800X at 3.80 GHz, 32-GB memory, and 64-bit Windows 10 operating system.

B. Results

First of all, setting the true squareness parameter to $\varepsilon = 4$ (non-convex diamond-like EO in Fig. 1), the result of a typical run of SE-EOT with $N = 500$ particles is shown in Fig. 3, where it can be seen that the proposed method can correctly perform EOT. In order to evaluate performance, let us define estimation errors for position e_p, velocity e_v, axis-lengths e_a, rotation angle e_α, and squareness parameter e_ε as follows:

$$e_p = \sqrt{\left(\xi_o - \widehat{\xi}_o\right)^2 + \left(\eta_o - \widehat{\eta}_o\right)^2},$$

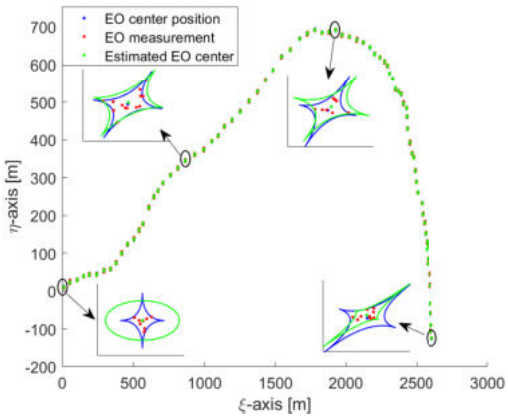

Fig. 3: Scenario and typical EOT trial with the proposed method, where true and estimated EO shapes are drawn in blue and green, respectively.

TABLE I: Average position and velocity estimation error.

Average error	Position $[m]$	Velocity $[m/s]$
SE-EOT	0.57	7.22
SE-EOT-Exact	0.57	7.21
MEM-EKF	0.59	7.23
RM-VB	0.58	9.83

$$
\begin{aligned}
e_v &= \sqrt{\left(\dot{\xi}_o - \widehat{\dot{\xi}}_o\right)^2 + \left(\dot{\eta}_o - \widehat{\dot{\eta}}_o\right)^2}, \\
e_a &= \sqrt{\left(a_\xi - \widehat{a}_\xi\right)^2 + \left(a_\eta - \widehat{a}_\eta\right)^2}, \\
e_\alpha &= |\alpha - \widehat{\alpha}|, \quad e_\varepsilon = |\varepsilon - \widehat{\varepsilon}|.
\end{aligned} \tag{31}
$$

Then, we also carried out 100 independent Monte Carlo trials and compared the RMSEs for both kinematic and shape states in Figs. 4 and 5, while time-averaged position and velocity estimation errors are reported in Table I. Please notice that the performance of exact likelihood based superellipse EOT (referred to as SE-EOT-Exact) with $N_s = 2000$ is also included to provide a comprehensive understanding of the proposed approximated likelihood.

As it can be seen, the proposed method has similar kinematic state estimation performance as MEM-EKF, while the proposed SE-EOT method and MEM-EKF slightly outperform RM-VB in velocity estimation. Besides, SE-EOT exhibits superior performance for shape estimation compared to both MEM-EKF and RM-VB. In particular, since the initial shape variables and their variances are such that the generated shape particles cover the region containing the ground-truth shape vector, the proposed algorithm features fast convergence. In contrast, since the extended object shape assumed by the MEM-EKF approach is severely mismatched with respect to the true shape of Fig. 3, axis length estimation performance is significantly deteriorated. Besides, it is also observed that the performance of SE-EOT is comparable to SE-EOT-Exact, thus verifying the effectiveness of proposed approximated likelihood. Since the SE-EOT-Exact is very time comsuming (in average 7.697 $[s]$ per iteration), it is not included in the following simulations.

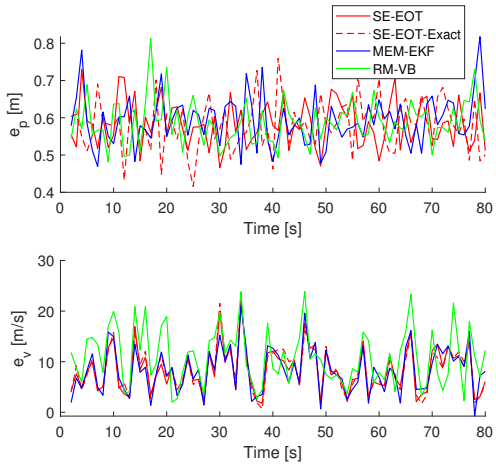

Fig. 4: Kinematic estimation performance for EO with $\varepsilon = 4$ (expected measurement number $\lambda_z = 10$ and $N = 500$ particles for SE-EOT).

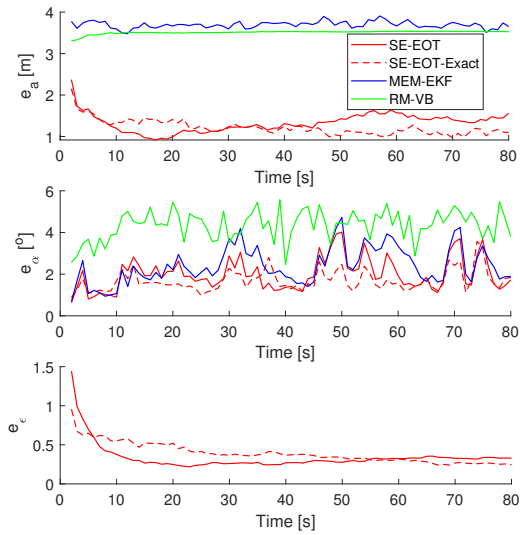

Fig. 5: Shape estimation performance for EO with $\varepsilon = 4$ (expected measurement number $\lambda_z = 10$ and $N = 500$ particles for SE-EOT).

In order to provide a comprehensive understanding of the proposed method, Table II reports its average performance and execution time under different numbers of particles and of expected measurements. It turns out that, though the proposed method takes longer execution time than MEM-EKF and RM-VB, its maximum execution time is anyway always less than $0.1[s]$, which is practically acceptable.

Then, we tested the performance of both algorithms on tracking an elliptical EO. For this test, we set the squareness parameter of SE-EOT to $\varepsilon = 1$. Since kinematic state estimation results of SE-EOT, MEM-EKF, and RM-VB have already been shown, only shape estimation results are provided in Fig. 6. It turns out that MEM-EKF yields better performance in estimating lengths of the axes and rotation angle of the

λ_z \ N	100	300	500	1000
5	SE-EOT: $1.419[m]$ ALE MEM-EKF: $3.774[m]$ RM-VB: $3.503[m]$ SE-EOT: $3.479[^o]$ RE MEM-EKF: $4.127[^o]$ MEM-EKF: $6.355[^o]$ SE-EOT: $3.685[ms]$ AET MEM-EKF: $0.277[ms]$ RM-VB: $0.597[ms]$	SE-EOT: $1.319[m]$ ALE MEM-EKF: $3.774[m]$ RM-VB: $3.503[m]$ SE-EOT: $3.637[^o]$ RE MEM-EKF: $4.127[^o]$ RM-VB: $6.355[^o]$ SE-EOT: $9.807[ms]$ AET MEM-EKF: $0.277[ms]$ RM-VB: $0.597[ms]$	SE-EOT: $1.253[m]$ ALE MEM-EKF: $3.774[m]$ RM-VB: $3.503[m]$ SE-EOT: $3.481[^o]$ RE MEM-EKF: $4.127[^o]$ RM-VB: $6.355[^o]$ SE-EOT: $15.558[ms]$ AET MEM-EKF: $0.277[ms]$ RM-VB: $0.597[ms]$	SE-EOT: $1.134[m]$ ALE MEM-EKF: $3.774[m]$ RM-VB: $3.503[m]$ SE-EOT: $1.795[^o]$ RE MEM-EKF: $4.127[^o]$ RM-VB: $6.355[^o]$ SE-EOT: $32.078[ms]$ AET MEM-EKF: $0.277[ms]$ RM-VB: $0.597[ms]$
10	SE-EOT: $1.111[m]$ ALE MEM-EKF: $3.652[m]$ RM-VB: $3.431[m]$ SE-EOT: $2.711[^o]$ RE MEM-EKF: $2.429[^o]$ RM-VB: $4.289[^o]$ SE-EOT: $6.442[ms]$ AET MEM-EKF: $0.399[ms]$ RM-VB: $0.912[ms]$	SE-EOT: $0.855[m]$ ALE MEM-EKF: $3.652[m]$ RM-VB: $3.431[m]$ SE-EOT: $2.090[^o]$ RE MEM-EKF: $2.429[^o]$ RM-VB: $4.289[^o]$ SE-EOT: $18.455[ms]$ AET MEM-EKF: $0.399[ms]$ RM-VB: $0.912[ms]$	SE-EOT: $0.835[m]$ ALE MEM-EKF: $3.652[m]$ RM-VB: $3.431[m]$ SE-EOT: $1.821[^o]$ RE MEM-EKF: $2.429[^o]$ RM-VB: $4.289[^o]$ SE-EOT: $30.333[ms]$ AET MEM-EKF: $0.399[ms]$ RM-VB: $0.912[ms]$	SE-EOT: $0.615[m]$ ALE MEM-EKF: $3.652[m]$ RM-VB: $3.431[m]$ SE-EOT: $1.363[^o]$ RE MEM-EKF: $2.429[^o]$ RM-VB: $4.289[^o]$ SE-EOT: $59.893[ms]$ AET MEM-EKF: $0.399[ms]$ RM-VB: $0.912[ms]$
15	SE-EOT: $0.824[m]$ ALE MEM-EKF: $3.640[m]$ RM-VB: $3.405[m]$ SE-EOT: $2.118[^o]$ RE MEM-EKF: $1.872[^o]$ RM-VB: $3.298[^o]$ SE-EOT: $9.440[ms]$ AET MEM-EKF: $0.540[ms]$ RM-VB: $1.271[ms]$	SE-EOT: $0.804[m]$ ALE MEM-EKF: $3.640[m]$ RM-VB: $3.405[m]$ SE-EOT: $1.462[^o]$ RE MEM-EKF: $1.872[^o]$ RM-VB: $3.298[^o]$ SE-EOT: $27.163[ms]$ AET MEM-EKF: $0.540[ms]$ RM-VB: $1.271[ms]$	SE-EOT: $0.680[m]$ ALE MEM-EKF: $3.640[m]$ RM-VB: $3.405[m]$ SE-EOT: $1.168[^o]$ RE MEM-EKF: $1.872[^o]$ RM-VB: $3.298[^o]$ SE-EOT: $44.618[ms]$ AET MEM-EKF: $0.540[ms]$ RM-VB: $1.271[ms]$	SE-EOT: $0.502[m]$ ALE MEM-EKF: $3.640[m]$ RM-VB: $3.405[m]$ SE-EOT: $1.156[^o]$ RE MEM-EKF: $1.872[^o]$ RM-VB: $3.298[^o]$ SE-EOT: $88.049[ms]$ AET MEM-EKF: $0.540[ms]$ RM-VB: $1.271[ms]$

TABLE II: Average estimation error and execution time statistics under $\varepsilon = 4$ (ALE: axis length error; RE: rotation error; AET: average execution time per iteration).

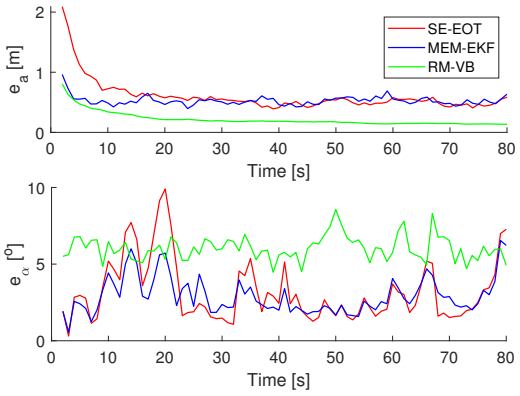

Fig. 6: Shape estimation performance for elliptical EO (i.e., $\varepsilon = 1$) under expected measurement number $\lambda_z = 10$ and $N = 500$ particles for SE-EOT.

elliptical EO at the beginning of the tracking process, then in the second half (i.e., after $50\,[s]$) the performance of SE-EOT tends to be slightly better with respect to MEM-EKF. In contrast, RM-VB outperforms SE-EOT and MEM-EKF in axis length estimation, while it exhibits inferior performance in orientation estimation.

As a last comparison, we set the squareness parameter of the EO to $\varepsilon = 0.5$ (nearly rectangular shape) and show the resulting shape estimation performance in Fig. 7. For better appreciating shape estimation accuracy, we compare true versus estimated shapes at time $t = 40\,[s]$ for a typical Monte Carlo trial in Fig. 8. As it can be seen, the proposed SE-EOT method turns out to be more accurate compared to MEM-EKF and RM-VB with respect to axis length estimation. Moreover, SE-EOT shows similar performance in orientation estimation compared to MEM-EKF, while RM-VB exhibits the worst orientation estimation performance.

It is worth noting that a superellipse with squareness $\varepsilon = 0.5$ is much closer to a rectangle than to an ellipse, so that rectangle-based modeling of the EO is expected to provide better shape approximation. However, please notice that the measurement model of MEM-EKF is developed based on a rectangular spatial distribution [10, Sec. B], and a rectangle can also be uniquely specified by semi-axis lengths and orientation angle, so that MEM-EKF can also be directly applied to rectangular EO tracking. From the above arguments, the effectiveness of the proposed SE-EOT method is further verified.

V. Conclusions

The problem of *extended object tracking* (EOT) has been considered in this paper. By representing the *extended object* (EO) as a superellipse, a suitable likelihood function, which considers the characteristics of the EO measurement generation, has been derived. Then, exploiting such a likelihood function, a superellipse-based EOT algorithm has been developed, where the kinematic state is estimated via a Kalman filter while shape estimation is accomplished via a particle filter. Simulation results have demonstrated the effectiveness of the proposed method. Future work will consider tracking of multiple EOs based on the superellipse model.

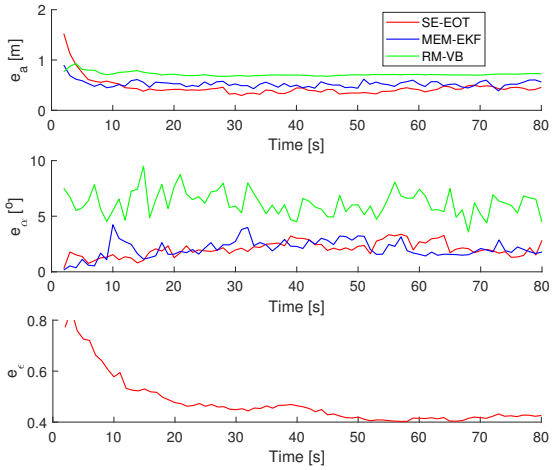

Fig. 7: Shape estimation performance for EO with $\varepsilon = 0.5$ (expected measurement number $\lambda_z = 10$ and $N = 500$ particles for SE-EOT).

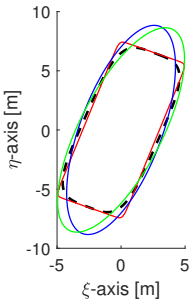

Fig. 8: True shape (dashed black) versus estimated shape obtained with SE-EOT (red), MEM-EKF (blue) and RM-VB (green) at time $t = 40\,[s]$ with $\varepsilon = 0.5$.

REFERENCES

[1] K. Granström, M. Baum, and S. Reuter, "Extended object tracking: Introduction, overview and applications," *arXiv preprint arXiv:1604.00970*, 2016.

[2] H. Alqaderi, F. Govaers, and R. Schulz, "Spacial elliptical model for extended target tracking using laser measurements," in *2019 Sensor Data Fusion: Trends, Solutions, Applications (SDF)*. IEEE, 2019, pp. 1–6.

[3] P. Broßeit, M. Rapp, N. Appenrodt, and J. Dickmann, "Probabilistic rectangular-shape estimation for extended object tracking," in *IEEE Intelligent Vehicles Symposium (IV)*, 2016, pp. 279–285.

[4] J. W. Koch, "Bayesian approach to extended object and cluster tracking using random matrices," *IEEE Transactions on Aerospace and Electronic Systems*, vol. 44, no. 3, pp. 1042–1059, 2008.

[5] M. Feldmann, D. Fräenken, and W. Koch, "Tracking of extended objects and group targets using random matrices," *IEEE Transactions on Signal Processing*, vol. 59, no. 4, pp. 1409–1420, 2010.

[6] U. Orgüner, "A variational measurement update for extended target tracking with random matrices," *IEEE Transactions on Signal Processing*, vol. 60, no. 7, pp. 3827–3834, 2012.

[7] J. Lan and X. R. Li, "Tracking of extended object or target group using random matrix: New model and approach," *IEEE Transactions on Aerospace and Electronic Systems*, vol. 52, no. 6, pp. 2973–2989, 2016.

[8] B. Tuncer and E. Özkan, "Random matrix based extended target tracking with orientation: A new model and inference," *IEEE Transactions on Signal Processing*, vol. 69, pp. 1910–1923, 2021.

[9] H. Alqaderi, F. Govaers, and W. Koch, "Bayesian Wishart filter for random shape tracking," *IEEE Transactions on Aerospace and Electronic Systems*, vol. 58, no. 3, pp. 1941–1952, 2021.

[10] S. Yang and M. Baum, "Tracking the orientation and axes lengths of an elliptical extended object," *IEEE Transactions on Signal Processing*, vol. 67, no. 18, pp. 4720–4729, 2019.

[11] K. Granström, P. Willett, and Y. Bar-Shalom, "An extended target tracking model with multiple random matrices and unified kinematics," in *18th International Conference on Information Fusion (Fusion)*. IEEE, 2015, pp. 1007–1014.

[12] N. Wahlström and E. Özkan, "Extended target tracking using Gaussian processes," *IEEE Transactions on Signal Processing*, vol. 63, no. 16, pp. 4165–4178, 2015.

[13] M. Baum, B. Noack, and U. D. Hanebeck, "Extended object and group tracking with elliptic random hypersurface models," in *13th International Conference on Information Fusion*, 2010, pp. 1–8.

[14] M. Baum and U. D. Hanebeck, "Extended object tracking with random hypersurface models," *IEEE Transactions on Aerospace and Electronic Systems*, vol. 50, no. 1, pp. 149–159, 2014.

[15] A. Zea, F. Faion, M. Baum, and U. D. Hanebeck, "Level-set random hypersurface models for tracking nonconvex extended objects," *IEEE Transactions on Aerospace and Electronic Systems*, vol. 52, no. 6, pp. 2990–3007, 2016.

[16] J. Yang, P. Li, and H. Ge, "Extended target shape estimation by fitting b-spline curve," *Journal of Applied Mathematics*, vol. 2014, 2014.

[17] X. Cao, J. Lan, and X. R. Li, "Extension-deformation approach to extended object tracking," *IEEE Transactions on Aerospace and Electronic Systems*, vol. 57, no. 2, pp. 866–881, 2020.

[18] L. Gong, S. Pathak, D. Haynor, P. Cho, and Y. Kim, "Parametric shape modeling using deformable superellipses for prostate segmentation," *IEEE Transactions on Medical Imaging*, vol. 23, no. 3, pp. 340–349, 2004.

[19] E. Dura, J. Bell, and D. Lane, "Superellipse fitting for the recovery and classification of mine-like shapes in sidescan sonar images," *IEEE Journal of Oceanic Engineering*, vol. 33, no. 4, pp. 434–444, 2008.

[20] P. Rosin, "Fitting superellipses," *IEEE Transactions on Pattern Analysis and Machine Intelligence*, vol. 22, no. 7, pp. 726–732, 2000.

[21] X. Zhang and P. L. Rosin, "Superellipse fitting to partial data," *Pattern Recognition*, vol. 36, no. 3, pp. 743–752, 2003.

[22] H. Kaulbersch, J. Honer, and M. Baum, "Assymetric noise tailoring for vehicle lidar data in extended object tracking", in *2020 IEEE International Conference on Multisensor Fusion and Integration for Intelligent Systems (MFI)*, 2020, pp. 191–196.

[23] Y. Xia, P. Wang, K. Berntorp, T. Koike-Akino, H. Mansour, M. Pajovic, P. Boufounos, and P. Orlik, "Extended object tracking using hierarchical truncation measurement model with automotive radar", in *2020 IEEE International Conference on Acoustics, Speech and Signal Processing (ICASSP)*, 2020, pp. 4900–4904.

[24] N. Gordon, B. Ristic, and S. Arulampalam, "Beyond the Kalman filter: Particle filters for tracking applications," *Artech House, London*, 2004.

[25] A. Jaklic, A. Leonardis, and F. Solina, "Segmentation and Recovery of Superquadrics," *Springer, Berlin*, 2000.

[26] Y. Li, K. Niklas, J. Gielis, Ü. Niinemets, J. Schrader, R. Wang, and P. Shi, "An elliptical blade is not a true ellipse, but a superellipse–evidence from two Michelia species," *Journal of Forestry Research*, vol. 33, pp. 1341–1348, 2022.

[27] W. Huang, Y. Li, K. Niklas, J. Gielis, Y. Ding, L. Cao, and P. Shi, "A superellipse with deformation and its application in describing the cross-sectional shapes of a square bamboo," *Symmetry*, vol. 12, no. 12, pp. 2073, 2020.

[28] L. Gong, S. Pathak, D. Haynor, P. Cho, and Y. Kim, "Parametric shape modeling using deformable superellipses for prostate segmentation," *IEEE Transactions on Medical Imaging*, vol. 23, no. 2, pp. 340–349, 2004.

[29] M. Osian, T. Tuytelaars, and L. Gool, "Fitting superellipses to incomplete contours," in *Conference on Computer Vision and Pattern Recognition Workshop*, 2004, pp. 49–49.

[30] P. Jia and J. Dannenhoffer, "Generation of parametric aircraft models from a cloud of points," in *54th AIAA Aerospace Sciences Meeting*, 2016, pp. 1–24.

[31] R. Kalman, "A new approach to linear filtering and prediction problems," *Journal of Basic Engineering*, vol. 82, no. 1, pp. 35–45, 1960.